

Revealing dynamical resonances of bars in PHANGS galaxies

Ruiz-García, M.¹, Querejeta, M.¹, García-Burillo, S.¹, and PHANGS.

¹ Observatorio Astronómico Nacional (IGN), C/Alfonso XII, 3, E-28014 Madrid, Spain

Abstract

Bars are remarkable stellar structures capable of transporting gas towards centers and drive the secular evolution of galaxies. In this context, it is important to locate dynamical resonances associated with bars. In this study, we use *Spitzer* near-infrared images as a proxy for the stellar gravitational potential and the ALMA CO(J=2-1) gas distribution from the PHANGS survey to determine the position of the main dynamical resonances associated with the bars in the PHANGS sample of 74 nearby star-forming galaxies. We use the gravitational torque method to estimate the location of the bar corotation radius (R_{CR}), where stars and gas rotate at the same angular velocity as the bar. Of the 46 barred galaxies in PHANGS, we have successfully determined the corotation (CR) for 38 of them. The mean ratio of the R_{CR} to bar radius is $\mathcal{R} = R_{\text{CR}}/R_{\text{bar}} = 1.12$, with a standard deviation of 0.39, consistent with the average value expected from theory and suggests that bars are predominantly fast. Finally, using the PHANGS rotation curves, we have estimated other relevant resonances such as the inner Lindblad resonance (ILR) and the outer Lindblad resonance (OLR), often associated with rings. This work provides a useful catalog of resonances for a large sample of nearby galaxies and emphasises the clear connection between bar dynamics and morphology.

1 Introduction

Galactic structures, such as bars, can drive galaxy evolution through the redistribution of gas. However, there are other non-gravitational mechanisms that also explain the radial redistribution of the gas, such as viscous torques and dynamical friction between large molecular clouds and stars (e.g., [6, 7, 17]). Bars are usually classified into slow bars or fast bars by studying the ratio between the corotation radius R_{CR} and the bar length R_{bar} , typically referred to as \mathcal{R} . [13] proposed fast present $1 < \mathcal{R} < 1.4$, while slow bars present $\mathcal{R} > 1.4$. Later, [5] and [1] added a new category to this classification. According to them, “ultra-fast bars” present $\mathcal{R} < 1$. This is the nomenclature we are going to follow hereafter.

In spiral galaxies, locations where the angular frequency Ω of a particle rotating with the disk is related to the angular frequency of the rotating pattern (e.g., bar) Ω_p as $\Omega = \Omega_p + \frac{l}{m}\kappa$ are known as dynamical resonances (see [3]). Examples of dynamical resonances are the corotation (CR) or the Lindblad resonances. At the CR we have that $\Omega(\text{CR}) = \Omega_p$.

These conference proceedings summarise the main results from [25]. In this work we study a sample of 74 galaxies, taken from the PHANGS-ALMA¹ survey (see [21]). Out of this sample, we have focused on those 46 galaxies that present bars. We use CO(2–1) maps and Near-Infrared (NIR) stellar mass maps from the PHANGS-ALMA and S⁴G survey² respectively. We study this subsample of 46 galaxies using the gravitational torques method (see [17]) to obtain their CR locations.

2 The gravitational torque method

Generally, torques are defined as $\tau = r \times F$, where r is the relative position of the particle with respect to the center, and F is the force exerted on the particles (i.e., the gravitational force acting on molecular gas). For τ to be non-zero, the force creating it must have a non-radial component. This is why non-axisymmetric potentials (such as those of barred galaxies) are needed to be able to apply the gravitational torques method. For more details on the method, we refer the reader to [17]. This method informs us about the expected redistribution of the angular momentum of the gas in a galaxy.

We need a combination of molecular gas observations and stellar mass maps to quantify the effect gravitational torques have on molecular gas. Images with high spatial resolution ($\sim 1''$, corresponding to ~ 100 pc in the PHANGS sample of galaxies) that trace the distribution of stars and gas are necessary for the accurate estimation of these phase shifts, as any offsets would be diluted otherwise.

Before obtaining the gravitational potential, the images are deprojected according to the inclination i and position angle PA of the galaxy using the code `pydisc`. Then, once the gravitational potential has been obtained (as explained in [17]), assuming steady state in the measured CO gas column density, we implicitly average over all possible orbits of gaseous particles and take into account the time spent by the gas clouds along the orbit paths. Thus, we compute the azimuthally averaged torques weighted by the present-day gas distribution to obtain $\tau(R)$. This is done by an integration of pixels in an annulus defined as $[R + \delta R]$, where $\delta R = 1.5$ arcsec.

We adopt the convention that $\tau < 0$ corresponds to gas inflow while $\tau > 0$ imply gas outflow. Thus, the sign of $\tau(R)$ will be affected by the sense of circulation of the gas. We assume a dextro-rotatory $[x, y, z]$ reference frame, therefore the sign of $\tau(R)$ is changed if the galaxy rotates clockwise, while the sign remains unchanged if the galaxy rotates counter-clockwise. We assign the signs based on the orientation of spiral arms, since all spirals in PHANGS are trailing (see [20]).

We locate the CR of the bar at the position in the disk where $\tau(R)$ changes its sign from

¹Physics at High Angular resolution in Nearby Galaxies

²*Spitzer* Survey of Stellar Structure in Galaxies

negative ($\tau(R) < R_{\text{CR}}$) to positive ($\tau(R) > R_{\text{CR}}$). Typically, the change of sign has to be present inside the radial range defined by $R_{\text{bar}} - 2R_{\text{bar}}$, with R_{bar} obtained from [24], as we do not anticipate to find the CR inside the bar according to classical theory [11, 10, 14]. The upper limit of this radial range is motivated by the previous findings in the literature, that obtain values in the range of $R \simeq (1.5 \pm 0.5)R_{\text{bar}}$. Nevertheless, we extend this interval further, considering that $\Delta = 0.25R_{\text{bar}}$ is a reasonable margin given typical uncertainties. Therefore, we search for the CR inside the range $0.75R_{\text{bar}} - 2.25R_{\text{bar}}$. We often find multiple zero crossings³ inside this range, so we associate the CR to the crossing presenting the largest amplitude. The amplitude is automatically calculated inside a range that spans from the previous to the following crossing⁴ as $\text{abs}(\tau_{\text{max}} - \tau_{\text{min}})$, where τ_{max} is the maximum $\tau(R)$ value reached within this range and τ_{min} the minimum value. This process is repeated for each galaxy.

3 NGC1097, case study

Here we present the case of NGC 1097, classified as strongly barred based on infrared data from [4, 23, 24, 26] (the latter classification is based on the clear bar lanes visible in the CO data). On the left panel of Fig. 1 we find the torque map of this galaxy. In its central part, we find a change of signs in the bar's consecutive quadrants, also known as butterfly pattern. Beyond the bar, on larger scales, we find another butterfly pattern that presents an orientation different than the first one. This scenario could be explained by the presence of a spiral structure with a different Ω_p than the bar (e.g., [16, 22]), resulting in a decrease of the positive torques associated with the bar. In this particular case of NGC 1097 we also find, as expected, negative torques along the leading sides of the bar.

In the upper central panel of Fig. 1 we present the CR location at $R_{\text{CR}} = 6.4$ kpc, showing a change from negative to positive torques. With a quick look at this panel, it is possible to find two more crossings from negative to positive within the range where we look for CR. However, their amplitude is smaller, so they are not chosen as the CR. Taking a look at the central region, at $R \sim 0.7$ kpc we see again a clear negative-to-positive crossing in $\tau(R)$, which could be indicative of an inner Lindblad resonance (ILR). This crossing could also be related to the presence of a ring. In fact, upon closer examination, we find a ring both in deprojected CO and deprojected $3.6 \mu\text{m}$ at $R \sim 10.4'' \sim 0.7$ kpc and $R \sim 13.6'' \sim 0.9$ kpc respectively, which is consistent with the results from [8], where $R_{\text{ring}} = 9.3 - 14.1''$ (deprojected).

On the lower central panel we can find a comparison with other estimations from the literature, using different methods, of R_{CR} . We obtain reasonable agreement between our estimation and those values and uncertainties.

³As bars are not isolated structures torque profiles may present some fluctuations due to the influence of other components, such as spiral arms.

⁴Regardless of whether these are negative-to-positive crossings or viceversa.

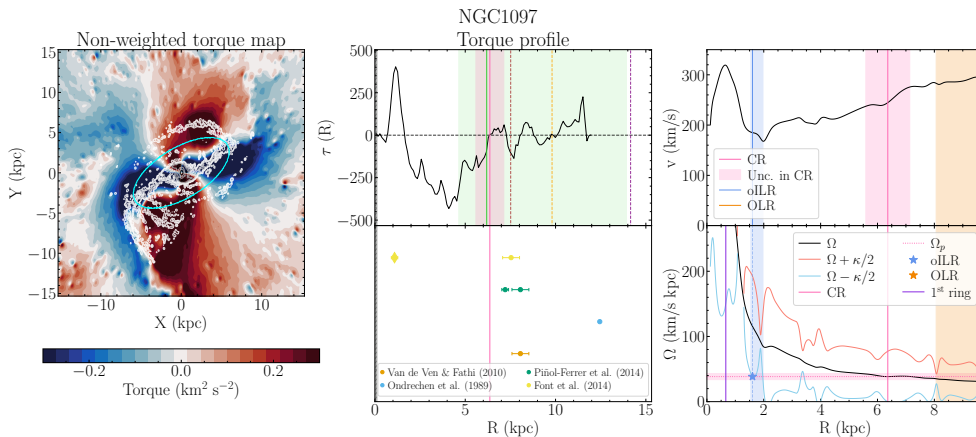


Figure 1: NGC 1097 non-weighted deprojected torque map (left panel), torque profile (upper central panel), comparison with values from the literature (lower central panel), rotation curve (upper right panel) and angular rotation curve (lower right panel). The cyan-contoured ellipse in the left panel indicates the bar extent. We show contours corresponding to $[5\sigma, 15\sigma, 45\sigma, \dots, 0.9\sigma_{\text{max}}]$ in the CO map, where σ is the mean value of the gas map. In the central and right panels, CR is represented as a vertical pink line, together with its uncertainties (pink-shaded area). The solid green line represents the bar length [24], while the shaded green region represents the region where we search for the CR. Finally, in the lower central panel, each dot represents a different measure of the CR (of the main bar) from the literature, and the diamond symbol represents a measure of a nuclear bar CR. For both right panels, the solid black line represents the rotation curve (left panel) and the angular rotation curve Ω (right panel). Solid light pink and light blue lines represent $\Omega + \kappa/2$ and $\Omega - \kappa/2$, respectively. The OLR and its uncertainties are represented in orange and the oILR (and its uncertainties) in dark blue. Purple vertical line represents the central ring detected by [24].

Finally, apart from CR, using the epicyclic theory, we can infer the inner Lindblad resonance (ILR) and outer Lindblad resonance (OLR) if we know Ω_p . First, from our derived R_{CR} , we estimate Ω_p as the intersection of the position of the R_{CR} and the angular velocity curve, since $\Omega = v/R$, obtaining $\Omega_p = 38.5 \pm 4.7 \text{ km s}^{-1} \text{ kpc}^{-1}$. Then, we calculate $\Omega \pm \kappa/2$ curves, where κ is the epicyclic frequency calculated as $\kappa^2 = R \frac{d\Omega^2}{dR} + 4\Omega^2$. For the case of a bar, $m = 2$, therefore $\Omega = \Omega_p \pm \kappa/2$. The intersection of $\Omega \pm \kappa/2$ with Ω_p provides the location of the ILR and OLR, respectively. Thus, the inferred position of ILR and OLR depend on the derivative of the rotation curve, which makes results highly sensitive to local wiggles. We find an outer inner Lindblad resonance (oILR) at $R = 1.0 \text{ kpc}$ and an OLR at $R = 9.6 \text{ kpc}$.

4 Fast bars vs slow bars

In [25], we obtain Fig. 2, which shows the distribution of \mathcal{R} for the whole sample, excluding those galaxies with a non reliable quality flag (QF), i.e., $QF = 3$. We find a mean value of $\mathcal{R} \sim 1.12 \pm 0.39$. With a quick look at Fig. 2, it can be seen that there is a majority of fast

bars (or bars compatible with the fast regime within their uncertainties), which aligns with some other studies such as [19, 12, 18]. From these 20 galaxies ($QF = 1, 2$), we found four galaxies (20%) with slow bars, six galaxies (30%) presenting fast bars, and 10 galaxies (50%) presenting ultra-fast bars, but in six of these cases, the galaxies are close to the transition line between these two regimes of $\mathcal{R} \sim 1$. However, [11, 10, 9] argue against the existence of ultra-fast bars ($\mathcal{R} < 1$), as in the classical theory, a bar cannot go beyond its CR.

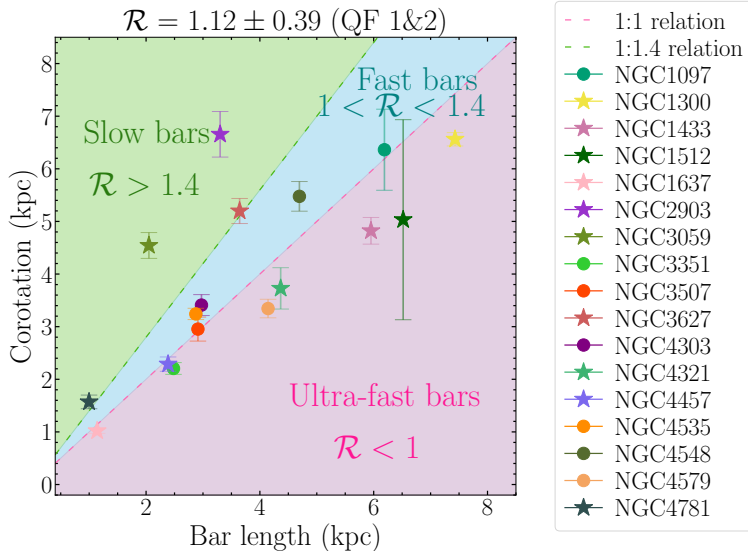


Figure 2: Slow, fast and ultrafast bars containing exclusively galaxies with $QF = 1$ (dots) and $QF = 2$ (stars).

The mean value of \mathcal{R} could suggest that bars do not suffer much dynamical friction by dark matter haloes ([15]). Alternatively, it can suggest that bars do slow down via dynamical friction at the same time they grow in mass and length over time, evolving with $\mathcal{R} \sim 1$ ([2]).

In [25] we also make a detailed comparison between our results and other measurements of R_{CR} estimated through different methods (e.g., Tremaine-Weinberg method, offset method, comparison to hydrodynamical simulations). We obtain a Spearman coefficient $\rho = 0.64$ (p -value < 0.001), which indicates a moderate positive relationship between our CR measurements and the ones from the literature, and a high significance of such correlation. We also compare all results from literature to other CR measurements, to study how well they correlate to one another.

Acknowledgments

MRG, MQ and SGB acknowledge support from the Spanish grant PID2022-138560NB-I00, funded by MCIN/AEI/10.13039/501100011033/FEDER, EU. This paper makes use of the following ALMA data: ADS/JAO.ALMA#2012.1.00650.S, ADS/JAO.ALMA#2013.1.00803.S, ADS/JAO.ALMA#2013.1.01161.S, ADS/JAO.ALMA#2015.1.00121.S, ADS/JAO.ALMA#2015.1.00782.S, ADS/JAO.ALMA#2015.1.00925.S, ADS/JAO.ALMA#2015.1.00956.S, ADS/JAO.ALMA#2016.1.00386.S, ADS/JAO.ALMA#2017.1.00886.L,

ADS/JAO.ALMA#2018.1.01651.S. ALMA is a partnership of ESO (representing its member states), NSF (USA) and NINS (Japan), together with NRC (Canada), MOST and ASIAA (Taiwan), and KASI (Republic of Korea), in cooperation with the Republic of Chile. The Joint ALMA Observatory is operated by ESO, AUI/NRAO and NAOJ. The National Radio Astronomy Observatory is a facility of the National Science Foundation operated under cooperative agreement by Associated Universities, Inc.

References

- [1] Aguerri, J. A. L., Méndez-Abreu, J., Falcón-Barroso, J., et al. 2015, *A&A*, 576, A102
- [2] Athanassoula, E. 2003, *MNRAS*, 341, 1179
- [3] Binney, J. & Tremaine, S. 1987, *Galactic dynamics*
- [4] Buta, R. J., Sheth, K., Athanassoula, E., et al. 2015, *VizieR Online Data Catalog*, J/ApJS/217/32
- [5] Buta, R. J. & Zhang, X. 2009, *ApJS*, 182, 559
- [6] Combes, F. 2002, arXiv e-prints, astro
- [7] Combes, F. 2004, in *The Interplay Among Black Holes, Stars and ISM in Galactic Nuclei*, ed. T. Storchi-Bergmann, L. C. Ho, & H. R. Schmitt, Vol.222, 383–388
- [8] Comerón, S., Salo, H., Laurikainen, E., et al. 2014, *A&A*, 562, A121
- [9] Contopoulos, G. 1981, *A&A*, 102, 265
- [10] Contopoulos, G. 1980, *A&A*, 81, 198
- [11] Contopoulos, G. & Papayannopoulos, T. 1980, *A&A*, 92, 33
- [12] Cuomo, V., Lee, Y. H., Buttitta, C., et al. 2021, *A&A*, 649, A30
- [13] Debattista, V. P. & Sellwood, J. A. 2000, *ApJ*, 543, 704
- [14] Elmegreen, B. 1996, in *Astronomical Society of the Pacific Conference Series*, Vol. 91, IAU Colloq. 157: Barred Galaxies, ed. R. Buta, D. A. Crocker, & B. G. Elmegreen, 197
- [15] Fragkoudi, F., Grand, R. J. J., Pakmor, R., et al. 2021, *A&A*, 650, L16
- [16] García-Burillo, S., Fernández-García, S., Combes, F., et al. 2009, *A&A*, 496, 85
- [17] García-Burillo, S., Combes, F., Schinnerer, E., Boone, F., & Hunt, L. K. 2005, *A&A*, 441, 1011
- [18] Garma-Oehmichen, L., Hernández-Toledo, H., Aquino-Ortíz, E., et al. 2022, *MNRAS*, 517, 5660
- [19] Guo, R., Mao, S., Athanassoula, E., et al. 2019, *MNRAS*, 482, 1733
- [20] Lang, P., Meidt, S. E., Rosolowsky, E., et al. 2020, *ApJ*, 897, 122
- [21] Leroy, A. K., Hughes, A., Liu, D., et al. 2021a, *ApJS*, 255, 19
- [22] Meidt, S. E., Rand, R. J., & Merrifield, M. R. 2009, *ApJ*, 702, 277
- [23] Menéndez-Delmestre, K., Sheth, K., Schinnerer, E., Jarrett, T. H., & Scoville, N. Z. 2007, *ApJ*, 657, 790
- [24] Querejeta, M., Schinnerer, E., Meidt, S., et al. 2021, *A&A*, 656, A133
- [25] Ruiz-García, M., Querejeta, M., García-Burillo, S., et al. 2024, *A&A*, 691, A351
- [26] Stuber, S. K., Schinnerer, E., Williams, T. G., et al. 2023, *A&A*, 676, A113